3-23-2016

A Trans-Dimensional View of Drug Resistance Evolution in Multiple Myeloma Patients

Timothy Jacobson

A Trans-Dimensional View of Drug Resistance Evolution in Multiple Myeloma Patients

by

Timothy W. Jacobson

A thesis submitted in partial fulfillment
of the requirements for the degree of
Master of Science in Biomedical Engineering
Department of Chemical and Biomedical Engineering
College of Engineering
University of South Florida

Co-Major Professor: Ariosto Silva, Ph.D.
Co-Major Professor: Robert Frisina, Jr., Ph.D.
William Lee III, Ph.D.

Date of Approval:
March 21, 2016

Keywords: cancer, precision medicine, personalized therapy, drug sensitivity, decision support
system

DEDICATION

Dedicated in honor of the endless support provided to me by my friends and loved ones.

ACKNOWLEDGEMENTS

In recognition of the faculty and role models whom afforded ample time and energy in support of my dissertation. I would like to extend special thanks to Dr. Ariosto Silva, Dr. Robert Frisina, Jr., and Dr. William Lee.

TABLE OF CONTENTS

LIST OF FIGURES

ABSTRACT

Multiple Myeloma (MM) is a treatable, yet incurable, malignancy of bone marrow plasma cells. This cancer affects many patients and many succumb to relapse of tumor burden despite a large number of available chemotherapeutic agents developed for therapy. This is because MM tumors are heterogeneous and receive protection from therapeutic agents by the microenvironment and other mechanisms including homologous MM-MM aggregation. Therefore, therapy failure and frequent patient relapse is due to the evolution of drug resistance, not a lack of available drugs. To analyze and understand this problem, the evolution of drug resistance has been explored and presented herein. We seek to describe the methods through which MM cells become resistant to therapy, and how this resistance evolves throughout a patient's treatment history. We achieve this in five steps.

First we review the patient's clinical history, including treatments and changes in tumor burden. Second, we trace the evolutionary tree of sub-clones within the tumor burden using standard of care fluorescence in situ hybridization (FISH). Thirdly, immunohistochemistry slides are stained and aligned to quantify the level of environmental protection received by surrounding cells and plasma in the bone marrow microenvironment (coined environment mediated drug resistance score [EMDR]). The fourth analysis type is produced through a novel 384-well plate ex vivo chemosensitivity assay to quantify sensitivity of primary MM cells to chemotherapeutic agents and extrapolate these findings to 90-day clinical response predictions. In addition to direct clinical application in the choice of best treatment, this tool was also used to study changes in sensitivity of patient tumors to other drugs, and it was

observed that, upon relapse, in addition to developing resistance to the current line of therapy, tumors become cross-resistant to agents that they were never exposed to. Finally, MM-MM homologous aggregation is quantified to assess the level of drug resistance contributed by clustering of patient tumor cells, which causes upregulation of Bcl-2 expression and other resistance mechanisms[1].

The findings of such experimentation improve comprehension of the driving factors that contribute to drug resistance evolution on a personalized treatment basis. The aforementioned factors all contribute in varying degrees for unique patient cases, seven of which are presented in depth for this project. In summary: Environmental protection plays a critical initial role in drug resistance, which is followed by increase in tumor genetic heterogeneity as a result of mutations and drug-induced Darwinian selection. Eventually, environment-independent drug resistant sub-populations emerge, allowing the tumor to spread to unexplored areas of the bone marrow while maintaining inherited drug resistant phenotype[2]. It is our hope that these findings will help in shifting perspective regarding optimal management of MM by finding new therapeutic procedures that address all aspects of drug resistance to minimize chance of relapse and improve quality of life for patients.

CHAPTER 1: INTRODUCTION

Multiple Myeloma (MM) is an incurable cancer of the bone marrow. Despite many available treatment options, prognosis remains quite poor and relapse occurs in many patients[3]. This relapse is known to occur due to genetic mutations that can lead to high risk tumor subpopulations[4,5], changes in the tumor microenvironment[6,7], and changes in phenotypic interaction by MM-MM cell adhesion/interaction[8]. High-risk patients have a low median overall survival (<2 years) despite the approval of many new drugs. This suggests that the problem is not lack of drugs but our lack of knowledge of how tumors evade therapy and develop drug resistance. Our goal, therefore, is to delay the rate of evolution of drug resistance and increase patient survival by one order of magnitude, reaching a functional cure. We seek here to further quantify the mechanisms of drug resistance and assess how they evolve throughout the course of therapy. This project aims to quantify the evolution of drug resistance across sequential biopsies of seven patients with respect to genetic abnormality, ex vivo response prediction, EMDR, and homologous MM-MM adhesion. First, we seek to understand the genetic abnormalities that drive drug resistance evolution.

Complex and multiple chromosomal abnormalities present themselves in the plasma cells of MM[4,5,9]. MM karyotypes can be analyzed for these abnormalities by means of interphase fluorescence in situ hybridization (FISH), which can analyze the chromosomes of non-dividing cells[5,9-11]. FISH probes are utilized in pairs and primarily apply to studies of monosomies/ trisomies, changes in chromosomes 17 and 13, and translocations of the immunoglobulin heavy-chain locus. This is due to the high clinical risk of poor prognosis typically associated with these

abnormalities, including the translocations of 14q32 (IGH) and 11q13 (CCND1) which causes overexpression of CCND1 and cell cycle dysregulation, and IGH translocation with 4p16 (FGFR3) which causes overexpression of MMSET leading to apoptosis prevention[3,12-18]. There is an additional risk associated with a deletion of chromosome 13, which promotes clonal expansion and is associated with hypodiploid MM, though there is no one specific genetic consequence of alterations to this chromosome[12].

FISH tests for these high-risk abnormalities, and thus not all genetic abnormalities are portrayed in a FISH panel. In subsequent discussion of clonal dynamics, care must be taken to define what is meant by a clone. The term clone, as it is presented here, refers to an identical group of cells with respect to MM-FISH report results. It is unknown if these cells are truly identical in areas other than genetic mutation detectable by the FISH probes. The chromosomal abnormalities detected play a variety of roles in drug resistance through deregulation of crucial proteins as discussed above. However, analysis of FISH alone as an indicator of drug resistance in MM remains insufficient, as patients with the same genetic abnormalities commonly have different clinical results[19-21]. We expect this is due to a multitude of additional factors including therapeutic intervention, environment-mediated drug resistance (EMDR), and MM homologous aggregation.

Another way to assess the changes in drug resistance throughout a patient's treatment history is to utilize the ex vivo results of experiments we performed using primary patient cells. This 96-hour well plate experiment allows us to quantify the continuous viability of cells obtained through bone marrow aspirates at Moffitt Cancer Center[22]. Through computational techniques utilizing pharmacokinetic models published for therapeutic agents, extrapolation of dose response can yield accurate predictions of clinical response for individual patients. These

results may be used to analyze drug resistance upon relapse and shows strong patterns of cross-resistance across the panel of chemotherapeutic agents. This data, though based on phenotype, may be used in conjunction with genetic mutation information to glean further into the evolution of drug resistance in MM. However, there are further methods that may be employed to continue broadening the scope of analysis to this end.

Environment mediated drug resistance (EMDR) is a term used to describe the bone marrow (BM) microenvironment's promotion of cell survival to therapy, and consequent contribution to minimal residual disease, through a variety of soluble and adhesive factors[23-28]. One such physical factor, fibronectin (FN) is known to control survival and growth of MM cells[29]. FN has been determined to play a prominent role in growth and drug resistance control in MM due to the promoted secretion of the cytokine interleukin (IL)-6[24,29,30]. FN adhesion to MM cells causes activation of integrin heterodimers composed of integrins α4 or α5 and β1 through intracellular signaling via protein tyrosine kinases (PTK) and receptor PTK[31,32]. Here, we propose a metric to assess the level of EMDR in MM patients through co-localization of MM membrane-bound β1 integrins and FN using immunohistochemistry (IHC) and digital image analysis. This approach generates frequency distributions of the tumor burden and the degree of EMDR protection to which they are submitted. If EMDR is a clinically relevant mechanism, sequential biopsies should depict changes in these levels in accordance with increases in drug resistance.

In addition to extracellular matrix- and stroma-derived factors, homologous (cell-cell) adhesion also promotes drug resistance in hematologic tumors[1,33]. The formation of aggregates among tumor cells (via 1.5% agarose solution in 96-well plates) has been shown to promote resistance to drugs including Bortezomib and Doxorubicin through an increase in the level of

3

Bcl-2, an anti-apoptotic protein[1]. Additionally, in solid tumors, the density of cell clusters poses a barrier to drug penetration by affecting magnitude of diffusion gradients that improves drug resistance with the formation of more compact, less invasive tumors[33-36]. Concurrently, the case of decreased cell proliferation in multicellular spheroids of pancreatic cancer has been shown to improve drug resistance through associated cascades in cell survival signaling, including cyclin-CDK (cyclin-dependent kinases), which regulates progression through the cell cycle and allows DNA injuries and chromosomal defects to be repaired[37-39]. The progression of tumor clustering throughout patient treatment has also been observed in MM[40]. A known cause of MM clustering is the expression of β-catenin that stimulates overexpressed signaling of Wnt, a paracrine growth factor that can influence MM growth[41,42]. It has been determined that N-cadherin is consequently over-expressed as the extracellular counterpart to β-catenin, and patient primary cells with high expression of CDH2 (the gene that encodes N-cadherin) correlates with a high probability (>83%) of high-risk genetic abnormalities such as t(4;14)(p16;q32) translocations and CCND1 (11q13) duplication, though the cause of the correlation between these two mechanisms of drug resistance remains unknown[43,44]. These abnormalities suggest poor prognosis for MM patients, and further strengthens the correlation between homologous adhesion of MM cells and drug resistance. Analysis of primary MM cell clustering due to MM-MM adhesion can provide additional insight into the evolution of drug resistance in patients.

4

CHAPTER 2: MATERIALS AND METHODS

2.1 Human Subjects/Clinical History

Redacted patient histories were obtained through the Total Cancer Care (TCC) Initiative at Moffitt Cancer Center. Name, age, and gender were removed from provided data to comply with anonymity of patients from researchers. However, blood test results showing tumor progression through serum free light chain (SFLC) and M-spike levels, as well as biopsy dates and therapeutic regimen utilized were all provided kindly by the Moffitt hospital.

2.2 Cell Lines and Primary Cell Protocols

Our previous work delves greatly into the procedures through which cell lines and primary patient cells were obtained and utilized ex vivo[45]. H929 and MM1s MM cell lines were cultured and utilized as positive control in ex vivo protocols. Primary cells from patients were obtained through the TCC initiative and magnetic bead sorted to select for CD138^{+} primary MM cells.

2.3 Ex vivo Procedures and Imaging

Additional work we have compiled and published in the Silva laboratory divulge great detail in the seeding of cells ex vivo, the equipment utilized, and the software composed in house to extrapolate experiment therapy response to clinical prediction[46]. Primary cells/cell lines are seeded in a 384 well plate with collagen and patient stroma to replicate the bone marrow microenvironment. Once incubated and spun to the same focal plane, drugs at relevant densities

5

(up to 31 plus control) were added to the plate and time-lapse imaging was run for 96 hours (image acquisition every 30 minutes). These results were then extrapolated to determine maximum tumor burden levels at 90-day clinical response for each patient utilizing pharmacokinetics and parameterization of evolutionary models with ex vivo results.

2.4 FISH and Phylogenetic Analyses

FISH reports are provided in a revised format by the Moffitt Cancer Center. First, we determine which probe results are abnormal from the Specific Probe Results report section, and which ones are mutually exclusive of each other based on chromosomal location. Care must be taken to realize that some abnormal results without translocation may simply be artifacts of a different probe analysis since they are always done in pairs. From the principle of maximum parsimony we expect that clonal dynamics of the tumor will follow the most 'straight-line' path in terms of the phylogenetic tree. This also suggests a much more increased likelihood of additional mutations presenting themselves stepwise through time, rather than the appearance and disappearance of multiple abnormalities from subpopulations. We compare FISH reports from sequential patient biopsies and create the tree based on these principles rather than chronological emergence. The results are an understanding of the percentage of tumor burden over time that contains the high-risk abnormalities tested in FISH and the phylogenetic tree of these abnormal clone subpopulations. If these principles are not followed in clonal dynamic determination, phylogenetic trees and subsequent results become overcomplicated and unclear. A detailed diagram for proper FISH report analysis is presented in Figure 2.1.

2.5 EMDR Score Determination and Calculation

EMDR score is based on bone marrow immunohistochemistry. Slides are requested and provided by the Moffitt Tissue Core for integrin β1, FN, and CD138 with corresponding positive and negative controls. All provided slides are scanned by the Moffitt Cancer Center Microscopy Core at up to 20x magnification and cropped and aligned manually to the best of the user's ability in ImageJ. Our macro takes the slides and completes their alignment to overlay pixels of each subsequent slide. The CD138 threshold value is determined based on the positive control slide and the average value of all negative control slides is stored as a noise mitigation constant to be subtracted from all future images. The aligned CD138 image is turned into a mask of zeros and ones, so that only myeloma-containing areas have numerical value. The FN and β1 8-bit images are overlaid and multiplied by the CD138 mask to allow for a maximum value of 65,025. The square root of this data set (maximum value of 255) is the EMDR score. In addition to this score, algorithms utilizing nearly identical processes are run to create the scores of FN and β1 in their respective slides, including areas with and without MM (CD138) and the slide as a whole. A detailed diagram of the EMDR computational process is presented in Figure 2.2.

2.6 Cluster/Aggregation Determination

The clustering of MM cells from patient primary samples is analyzed throughout patients' histories to further explore mechanisms of drug resistance. Four replicate images of control wells from the aforementioned ex vivo assay[46] at time point zero, imaged in phase contrast at 5x magnification, are saved and quantified to determine the number of neighbors that each live cell has within a 20-pixel diameter. This diameter was chosen with care to ensure a window that is large enough to capture multiple cells, but not large enough to count cells that are

7

un-clustered or far apart. The typical MM patient primary cell is 5-8 pixels in diameter. The mean number of neighbors for each cell in the well is a straight forward and accurate way to quantify the phenotypic clustering that can occur in patient samples (such as in case 2). In supplementation of these results, a cohort of 11 patients were quantified for number of neighbors and plotted versus the sum of the area under the curves from our ex vivo assay (Silva et al. *In review*). A graph is synthesized for each drug in this manner to determine if any linear correlation exists between therapy resistance and the phenotypic clustering we seek to further understand.

2.7 Chapter Two Figures

Initial Report Analysis
- From MM-FISH Reports, determine what abnormalities are present across patient biopsies.
- Determine which biopsies must be mutually exclusive based on chromosomal location.

Abnormalities to clones
- Following the principle of maximum parsimony, expect the most 'straight-line' path of genetic mutation, realizing that emergence is more likely to be based on complexity rather than chronology.
- Group the tumor burden by percentage across the biopsies to determine the most likely mutation paths.

Phylogenetic Tree Synthesis
- Label these clones and map the phylogenetic tree that most likely represents the FISH report in its entirety.
- Note that unknown percentages are not necessarily normal, they are untested by standard of care FISH probes.
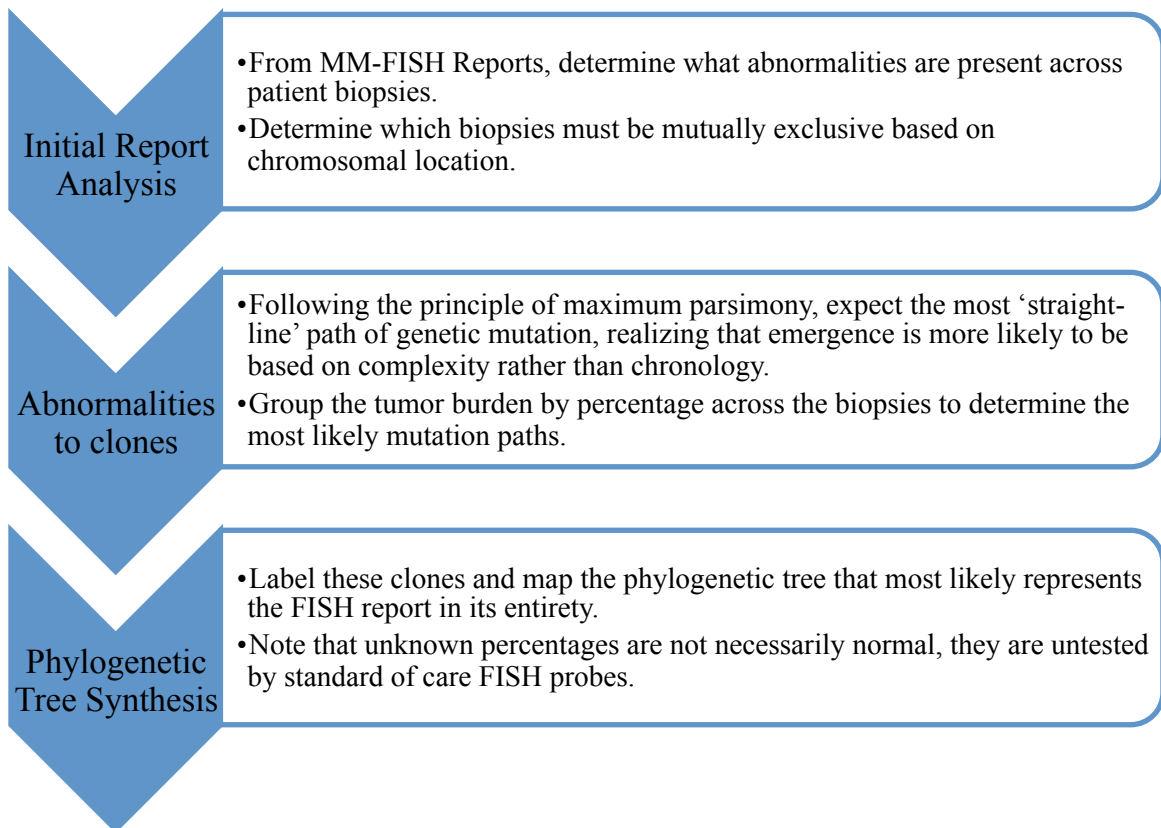
Figure 2.1: Flow of Information: FISH Report Analysis. Flow of information for analysis of FISH reports and determination of phylogeny of tumor subpopulations for each patient and the extrapolation of this information to determine clonal dynamics.
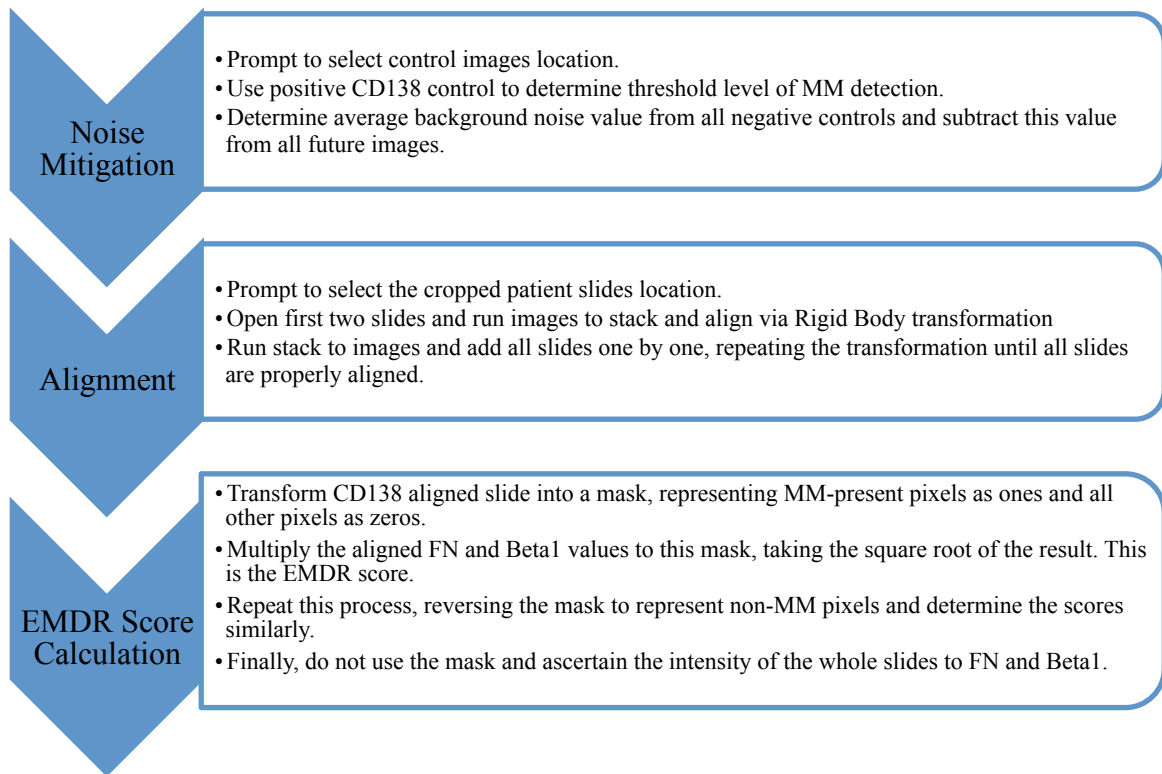
Noise Mitigation
- Prompt to select control images location.
- Use positive CD138 control to determine threshold level of MM detection.
- Determine average background noise value from all negative controls and subtract this value from all future images.

Alignment
- Prompt to select the cropped patient slides location.
- Open first two slides and run images to stack and align via Rigid Body transformation
- Run stack to images and add all slides one by one, repeating the transformation until all slides are properly aligned.

EMDR Score Calculation
- Transform CD138 aligned slide into a mask, representing MM-present pixels as ones and all other pixels as zeros.
- Multiply the aligned FN and Beta1 values to this mask, taking the square root of the result. This is the EMDR score.
- Repeat this process, reversing the mask to represent non-MM pixels and determine the scores similarly.
- Finally, do not use the mask and ascertain the intensity of the whole slides to FN and Beta1.

Figure 2.2: Flow of Information: EMDR Analysis. Algorithmic procedure for determining EMDR score for each patient biopsy. This outline is designed to contribute to holistic understanding of the ImageJ macro, as all steps once run are automatic.

CHAPTER 3: RESULTS

3.1 Clinical Relapse is Followed by Tumor Population Turnover

Analysis of tumor phylogeny across patient clinical history provides insight into the development and progression of tumor cell heterogeneity and drug resistance. The case shown in Figure 3.1 presents a patient treated over nearly 80 months (case 1). The serum free light chain (SFLC) measurement throughout the course of treatment is presented with therapy regimen in panel A. Four sequential relapse events occur between bone marrow biopsy (BMBx) 1 and 7, with a sharp relapse spike in SFLC from BMBx 7 to 8 that remains relatively consistent through the remaining two biopsies (9 and 10). MM-FISH reports from these biopsies may be analyzed and interpreted to generate clonal dynamic and phylogenetic tree representations.

This patient has a fairly complex phylogenetic tree (Figure 3.1C). Starting from clones 1 through 3, subsequent clones contain the same abnormalities as their predecessors with additional mutations, creating more complex tumor subpopulations. For example, from clone 1.1 to 1.2, an additional translocation of 11q and 14q presents itself, and from clone 3.2 to 3.2.1, a deletion of the 14q chromosome appears. Clonal dynamics seen in Figure 3.1B appear minimal until bone marrow biopsy (BMBx) 8, which is matched by a sharp spike in tumor burden (Figure 3.1A). From this point onward, more complex clones tend to take the place of their 'parent' clones. This behavior can also be seen in cases 3 and 4 (Supplemental Figures A.5 and A.7 respectively).

Case 3 has a steadily increasing tumor burden that is accompanied by clonal dynamic shifts. We see from Figure A.5F that the phylogeny is one straight line, and Figure A.5D shows

that from BMBx1 to 3, clone 1.1 is steadily overtaking clone 1, and clone 1.1.1 emerges rapidly between biopsies 2 and 3. Case 4 shows similar results (Figure A.7D). From BMBx1 to 2, clone 1 is overtaken by daughter clones 1.1 and 1.2. From BMBx 2 to 3, clone 1.1 remains present while clone 1.2.1 begins to overtake its parent clone (clone 1.2). Case 7 represents a straightforward phylogeny with only one clone containing one abnormality (Supplemental Figure A.11). From BMBx 2 to 4 in this case, while undergoing no treatment, the tumor appears to relapse slowly with a concurrent growth rate of clone 1, suggesting that these cells have some sort of survival advantage over the non-mutated remainder. Case 5 presents an interesting phenomenon of reemergence of a previously undetected parent clone (Supplemental Figure A.8). In fact, clone 1 is not detected until BMBx4, while daughter clones portray expected behavior in the first two biopsies. This is also seen in Figure 3.1 with respect to Clone 1.

3.2 Chemotherapeutic Intervention Can Lead to Cross-Resistance for Subsequent Therapy

From panels A, C, and E of Figure 3.2 we see that between biopsies 8 and 10, despite the lack of a significant tumor burden change, the predicted tumor burden decrease is significantly higher for Bortezomib, Melphalan, and CRM1i. This cross-resistance occurs while the patient is treated with TH-302, Bortezomib, and Dexamethasone. From panels B, D, and F, we see there is treatment between biopsies 3 and 5 of TH-302, Bortezomib, and Dexamethasone as well, however there is an increase only in Melphalan resistance. This suggests that treatment given does not result in similar resistance changes for different patients. However, it is important to note that in all cases encountered during which resistance evolves, there is a marked increase in resistance to drugs that patients have not been exposed to, suggesting that resistance occurs by mechanisms that are not unique to one or even a few particular drugs.

11

3.3 Environmental Protection Changes with Tumor Burden and Cell Location

Analysis of EMDR can provide insight into the extent and progression of environmental protection MM cells are receiving throughout patient therapy. References to FN score and $\beta 1$ score refer to the CD138-positive regions (blue lines). Figure 3.3 represents a case (case 2) for which patient response was tracked over nearly 40 months with tumor burden measured using sM-spike (Figure 3.3A). We see a steady increase in disease progression from BMBx1 to 3 with a sharper increase from BMBx 3 to 4, leveling out by BMBx 5. It is observed that EMDR score (Figure 3.3B) increases from BMBx1 to 2, and decreases from BMBx2 onward. FN and $\beta 1$ scores share the same behavior (Figure 3.3B and 3.3C respectively), though FN score decreases to a greater extent, falling below even the healthy tissue expression levels. This trend of EMDR score increase during lower tumor burden levels and EMDR decrease during spikes in tumor burden is also present in Supplemental Figure A.1 (case 1), where EMDR is consistently increasing until BMBx 8 at which point there is a dramatic raise in SFLC level. For the remaining two biopsies, EMDR score decreases. Cases 3, 4, and 5 show no significant change in EMDR score across sequential biopsies (Supplemental Figures A.5, A.7, and A.8).

3.4 Alternative Mechanisms of Resistance: Clustering

After analysis of clonal dynamics and EMDR for several cases, we noticed that when compared to our ex vivo results, the variability in cross resistance and sensitivity to drugs varied between cases 1 and 2, despite being on the same course of treatment (TH302/BTZ/DEX). We expect, therefore, that there is another mechanism of drug resistance left to explore. In further analysis of the ex vivo results, we took a look at the images utilized in patient response prediction and observed an increase in clustering of MM patient cells in case 2, but not in case 1.

12

Based on this finding, we developed a novel 'number of neighbors' algorithm to quantify the phenotypic change of patient cell locations and clustering once seeded in the 384-well plate. Cases 1 and 2 are represented in Figure 3.4A-D. Case 1 (Figure 3.4A and C), from BMBx 8-10 had previously shown a dramatic spike in tumor burden, and stays relatively constant during this time. The FISH clones appear very complex and show complete population progression of subpopulations with more chromosomal abnormalities. The ex vivo results for case 1 show dramatic increase in resistance to both Melphalan and Bortezomib from BMBx 8 to BMBx 10 (Figure 3.2C and E). EMDR begins decreasing over this time period as well (Supplemental Figure A.1). Clustering of MM primary cells during this time frame, however, appear stagnant and minimal. The same is observed in case 3, however the tumor burden in this case is continuously increasing from BMBx 1 to 4 (Supplemental Figure A.5A and A.6), with less dramatic but still significant change in FISH dynamics as clone 1.1 overcomes clone 1 and clone 1.1.1 emerges as the most fit genetic variation. In case 3, EMDR remains constant across all biopsies (Figure A.5) and according to ex vivo results (Figure A.6), there is an increased sensitivity to Melphalan and a steady increase in resistance to Carfilzomib.

In contrast to cases 1 and 3, cases 2 and 6 (Figures A.4 and A.10 respectively) show significant increase in clustering across sequential biopsies. While FISH, ex vivo, and EMDR results are unavailable for case 6, we see a response to drug, followed by relapse between biopsies one and two, which is accompanied by an increase in MM-MM cell adhesion. For case 2, we see an increase in tumor burden, decrease in EMDR, and increase in Melphalan resistance between BMBx3 and 5. FISH progresses with the emergence and successful growth of clone 1.1.2 and clustering appears to gradually increase across this time window.

13

Utilizing the 'number of neighbors' algorithm to quantify clustering phenotype across 11 different patients exposed to 25 PKI's in the 384-well plate ex vivo study (Silva et al In Review) allowed correlations to be determined between cell survival in the experiment (AUC %) and the mean number of neighbors for that well (Figure 3.4). A statistically significant non-zero slope shows such a correlation, which was present in two drugs in the panel, Melphalan and Linifanib. Significance of these findings suggests a phenotypic clustering mechanism of survival in response to these two chemotherapeutic agents. The remaining drugs showed a slope that did not significantly differ from zero, signifying that, although mechanisms of drug resistance may exist for these agents, MM-MM adhesion displays no indication of being one such mechanism.

3.5 Chapter Three Figures
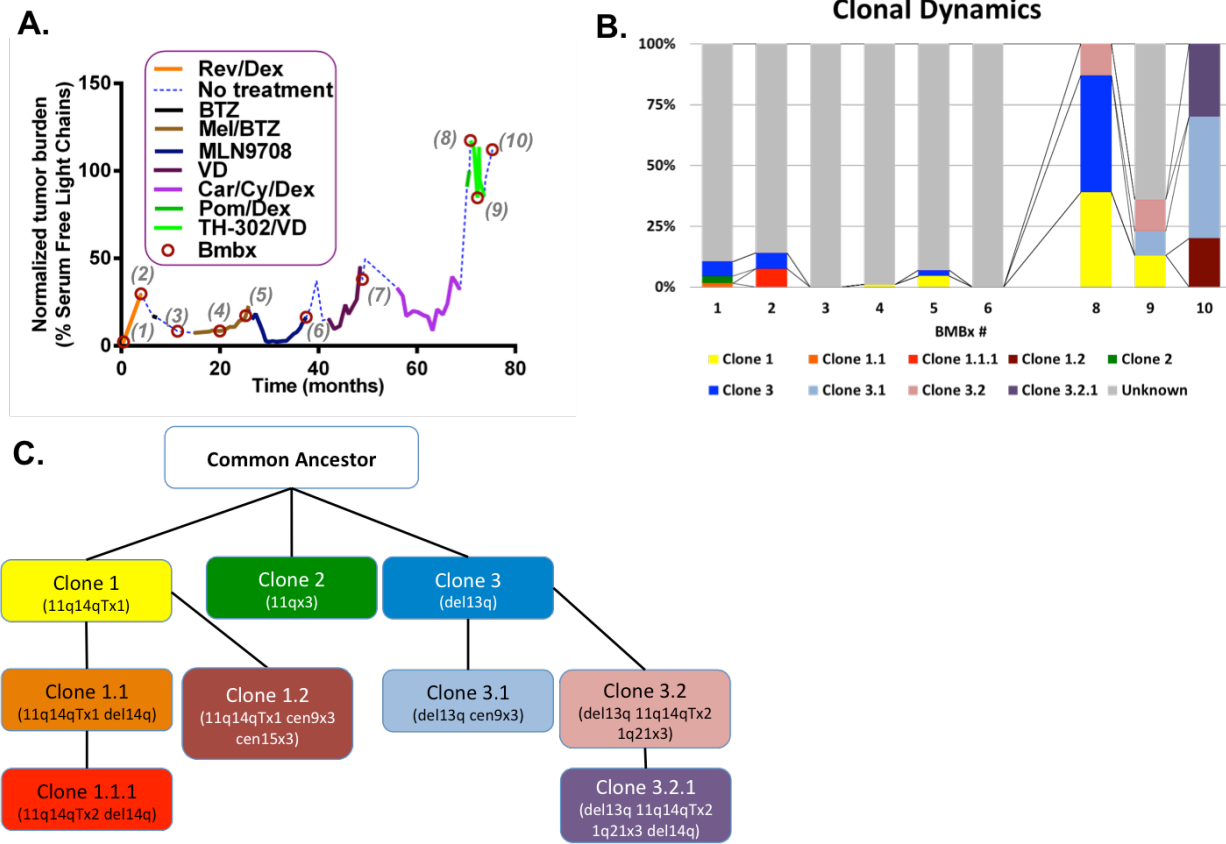
Figure 3.1: Case 1 Patient History, Phylogenetic Tree, and Clonal Dynamics. A) Clinical Patient History based on Serum Free Light Chain measurements over a period of time in months. Biopsies are labeled and noted by red circles, with plot colors corresponding to the therapeutic regimen shown in the key. B) Clonal dynamics developed using FISH reports across sequential biopsies. After abnormalities in each biopsy are analyzed and clonal results discovered, they are plotted as a column plot representing the appropriate percentage of tumor cells that make up each genetically mutated subpopulation. C) A phylogenetic tree is synthesized to further describe the clones present in panel B. These clones are listed with the abnormalities displayed beneath and are constructed based on the principle of maximum parsimony, understanding that increases in heterogeneity and complexity occur chronologically, while varying percentages given in FISH reports represent abnormalities present that may not be mutually exclusive between clonal subpopulations. We see here that as tumor burden increases toward biopsies eight through ten, the genetic abnormalities become increasingly complex and represent a larger population of the tumor burden. (Case 1)
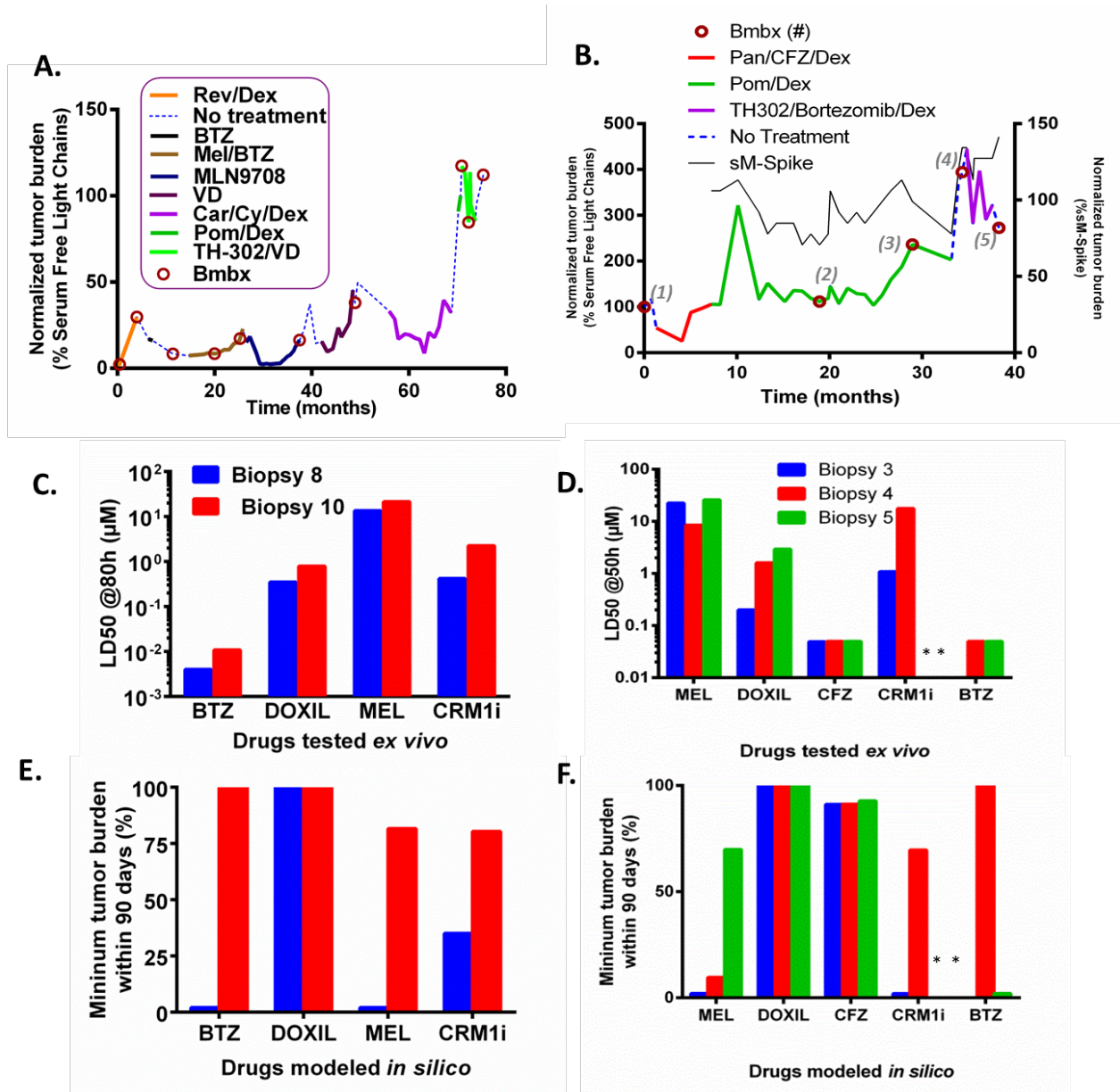
Figure 3.2: Case 1 and 2 Clinical History and Response Predictions. A-B) Patient clinical history with tumor burden determined via SFLC. Biopsies are denoted by open circles and colored lines correspond to therapeutic agents shown in the legend. C-F) Ex vivo chemosensitivity determined across patient biopsies for several drugs with known pharmacokinetics. Panels C and D show the LD50 of each drug across treatment and panels E and F represent the minimum tumor burden expected within 90 days after computational modeling of patient response. Panels A, C, and E represent case 1 and panels B, D, and F represent case 2.
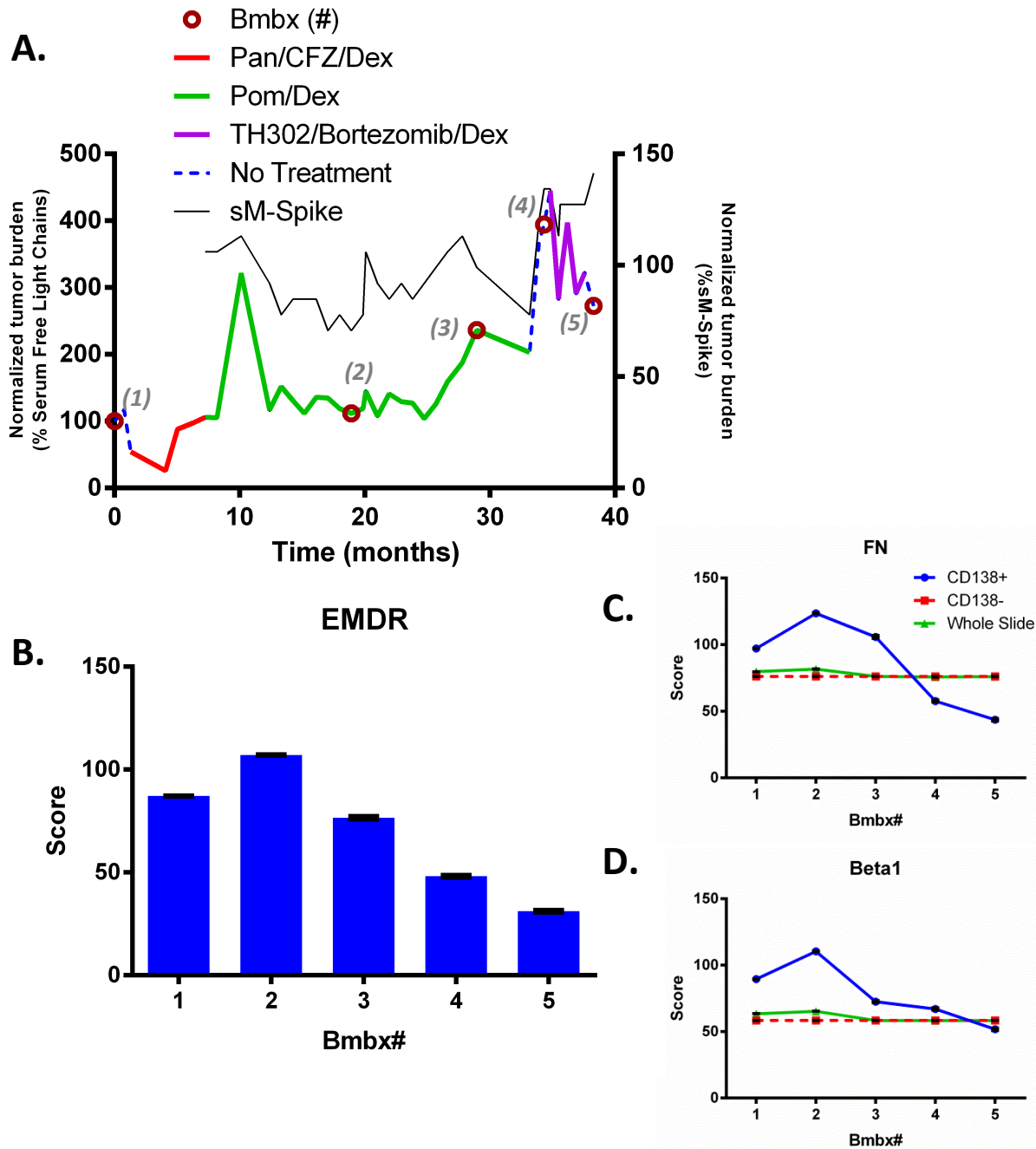
Figure 3.3: Case 2 Patient History, EMDR, FN, and Beta1 Scores. A) Patient clinical history based on M-spike measurements over a period of time in months. Biopsies are labeled and noted by red circles, with plot colors corresponding to the therapeutic regimen shown in the key. B) EMDR score based on a maximum value of 255 across patient biopsies. C) FN is scored independently in the CD138 positive and negative areas as well as the IHC slide as a whole. D) Integrin β1 scores are determined in the same manner as FN. All scores are normalized by CD138 negative region intensity. (Case 2)

| Drug Name	P value	R²	Pearson r
Linifanib (10µM)	0.039	0.3329	0.576975
MEL (50µM)	0.0447	0.3179	0.563826
Alisertib (10µM)	0.067	0.2729	0.522398
DOXIL (50nM)	0.2479	0.1192	0.345254
BMS777607 (10µM)	0.2506	0.3106	0.557315
PAN (50nM)	0.2778	0.1059	0.325423
Ruxolitinib (10µM)	0.2855	0.1028	0.320624
AZD1208 (10µM)	0.3087	0.09384	0.306333
BMS754807 (10µM)	0.3187	0.09021	0.30035
Selumetinib (10µM)	0.3697	0.07367	0.271422
AZD1480 (10µM)	0.3911	0.06755	0.259904
Dabrafenib (10µM)	0.4007	0.06495	0.254853
VX745 (10µM)	0.402	0.1798	0.424028
INK128 (10µM)	0.4125	0.06187	0.248737
Ralimetinib (10µM)	0.4557	0.1454	0.381314
Vemurafenib (10µM)	0.4604	0.1427	0.377757
Palbociclib (10µM)	0.4677	0.04892	0.221179
Motesanib (10µM)	0.489	0.0445	0.21095
CFZ (50nM)	0.5358	0.03581	0.189235
Momelotinib (10µM)	0.5577	0.03216	0.179332
Idelalisib (10µM)	0.6015	0.07419	0.272378
BTZ (50nM)	0.7274	0.0115	0.107238
Dasatinib (10µM)	0.7286	0.01139	0.106724
Ibrutinib (10µM)	0.7649	0.009355	0.096721
Ponatinib (10µM)	0.8115	0.005398	0.073471
BI2536 (10µM)	0.8127	0.005326	0.072979
MK2206 (10µM)	0.871	0.002505	0.05005
Tozasertib (10µM)	0.879	0.002201	0.046915
Trametinib (10µM)	0.9176	0.001018	0.031906
Crizotinib (10µM)	0.9998	5.18E-09	7.2E-05
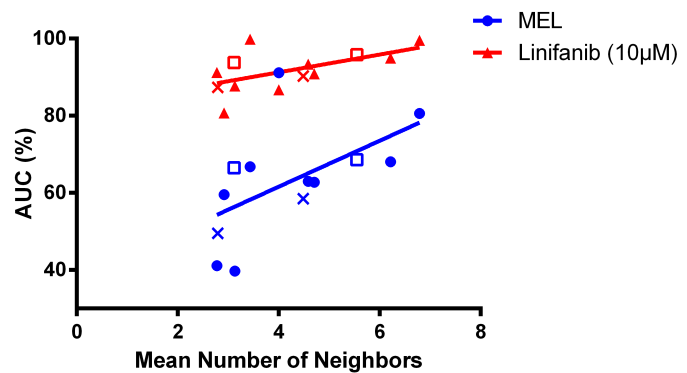
Figure 3.4: Case 1 and Case 2 Homologous MM-MM Adhesion and Clustering Analysis of Therapeutic Agents. A, B) Clustering, as determined by a 'number of neighbors' algorithm, is plotted with each dot representing a cell in the control well at time zero of the 384-well plate assay with mean and standard error as black line(s). C, D) Images of 384 well plate after patient cell seeding. Table) A cohort of 11 patients exposed to 25 PKI's was analyzed using the clustering analysis algorithm. A linear trend between resultant cell death in the 384 well plate ex vivo assay was compared to the mean number of neighbors seen at time zero in the control wells. P-values, R squared correlation coefficient, and Pearson r values are reported for each drug, with the two significantly non-zero sloped drugs, Melphalan and Linifanib, plotted (E). X's and squares represent two patients that underwent two sequential biopsies, both of which are plotted for both drugs, resulting in 13 final data points.

18

CHAPTER 4: DISCUSSION

4.1 Complex Genetic Mutation and Clonal Evolution as a Mechanism of Relapse and Cross-Resistance

Analyses in this chapter discuss the results of our work with respect to the different patient cases. Complete figures with all obtained data for these cases are present in the Supplemental Figures section of the Appendix. The specifics of high-risk genetic abnormalities as they pertain to drug resistance and therapy failure in MM have been well-explored[47]. However, the origins of these mutations in response to therapy, environmental factors, the effect of abnormality combinations, and the successful risk stratification based on these abnormalities remain particularly elusive in MM[13]. We see from the results of our phylogenetic trees and clonal dynamic determinations that although these mutations do in fact cause increased risk of relapse, the results are rarely equivalent regarding depth and duration of response (or lack thereof) and the development of cross-resistance to therapy. For example, in our cases 1 and 2, the patients were on the same therapeutic regimen of TH302, BTZ, DEX, both showed marginal response to the drug (BMBx8-10 in case 1 and BMBx4 to 5 in case 2), and both had over 90% presence of genetically abnormal clones. However, we see very little change in clonal dynamics for case 2 and a complete clonal extinction event in case 1 where all clones present in BMBx10 are 'daughter' clones of those present in BMBx8 with no trace of the 'parent' clones remaining. Also, in both of these time periods, ex vivo clinical predictions show varying cross-resistant tumors resulting from the therapy. Case 1 shows substantial increase in resistance to Bortezomib for which he/she was treated, but also a cross-resistance to Melphalan and CRM1i. In contrast,

19

case 2 showed development of cross-resistance to Melphalan, but an increased sensitivity to Bortezomib. Therefore, clinical therapeutic intervention decisions should not be based solely on genetic abnormality. Likewise, clonal dynamics is only one piece of the puzzle regarding drug resistance in MM.

Another point worth discussing is the observable evolutionary drive toward heterogeneity among tumor subpopulations instead of a bottleneck effect similar to BCR-ABL in chronic myeloid leukemia (CML)[48]. These speciation events most likely occur to improve the chance for survival of one of the clonal populations in the face of varying, dynamic therapeutic regimen. We can see from our results that once speciation leads to a superior clone in the face of a particular therapy, this clone grows very rapidly and overtakes other less fit clones as in case 2 with clone 1.1.2 between BMBx2 and 4, and case 5 with clone 1.1.1.1 between BMBx1 and 2.

4.2 Exploring the Inverse Trend Between Tumor Burden and EMDR

Human MM cells, when adherent to bone marrow stromal cells, increase IL-6 secretion[49]. IL-6 receptors in turn promote production of Janus kinase (Jak)/STAT3, which is known to increase survival of patient cells under therapeutic conditions[29,50-53]. Shain et al. demonstrated that when FN binds to the Integrin α4/β1 dimer on the MM cell surface, the STAT-3 pathway is further stimulated by increased IL-6 production as a result of preloading gp130. These concepts are further articulated by our findings regarding the EMDR score. In cases 1 and 2, as treatment progresses, EMDR score begins to rise. However, both cases also show that once tumor burden increases dramatically during relapse, the EMDR scores decrease.

We propose that this decrease is due to two primary factors. First, that ligation of integrin β1 on hematopoietic tumor cells can lead to arrest of the cell cycle[54-58]. And second, that there is

limited space in the perivascular niche of the BM, and as tumor burden increases to a size that is unsustainable within this area, cells must venture to less ideal locations with fewer stromal cells to promote IL-6 secretion. This also justifies why FN scores decrease at a more rapid rate than integrin β1 scores, since relocation of tumor cells away from stroma would have a more immediate effect on FN presence but a delayed decrease in integrin β1 levels in the MM cells. The rapid proliferation of tumor cells that causes this decrease in factors measured by EMDR score may be due in part to genetic evolution of more fit subpopulations as well as MM-MM cell interactions and clustering that create another mechanism of protection to certain treatments such as Melphalan and Linifanib, as mentioned in our results. In these cases, the surviving cells that do not contribute to EMDR score would grow faster and render the STAT3 pathway irrelevant to successful proliferation.

4.3 Possible Advantages of MM-MM Cell Adhesion to Drug Resistance

From clustering results across sequential patient biopsies, we see clearly the presence of MM cell clustering in two cases, while two others show no evidence of this phenotype at all. We propose that as EMDR score goes down and cells are forced to move to other areas of the bone marrow, clustering is one mechanism that promotes survival in the presence of chemotherapeutic agents. This is supported by a concurrent 'desire' for cells to become more genetically complex and improve resistance through this pathway. From the substantial correlation between high-risk genetic mutation and N-cadherin overexpression, the homologous adhesion of MM cells may contribute positively to genetic resistance as well[41,43]. This may help explain why in patients such as our Case 1, in which successfully developed complex genetic clones show an increased ability to survive therapy, the clustering phenotype has been circumvented, while in other cases

21

such as Case 2, MM-MM cell adhesion is a necessary step in survival when leaving the perivascular niche.

Clustering results across 13 samples (from 11 patients) showed correlation between MM-MM cell adherence and survival ex vivo while treated with Melphalan or Linifanib. Mechanisms of resistance to Melphalan in MM primary cells has been previously explored and significant findings relate cytogenetics, and adhesion to bone marrow stromal cells and FN to increased tumor survival while exposed to the drug[59,60]. MM-MM homologous interaction can further this drug resistance by means of cell cycle inhibition to allow improved DNA repair caused by alkylating agents[43,61]. As an ATP-competitive tyrosine kinase inhibitor, Linifanib is effective against active FMS-like receptor tyrosine kinase 3 (FLT3), other platelet derived growth factor receptors, and vascular endothelial growth factor receptors[62]. In vitro, Linifanib has caused inhibition of several downstream pathways of FLT3, including the Jak/STAT pathway and cell cycle regulators like Cyclin D and p27k[63,64]. However, no previous findings have been made relating MM cell aggregation to Linifanib drug resistance.

4.4 Summary of Findings

A summary of our findings is represented in Figure 4.1. This figure shows a representation of our proposed schematic of drug resistance evolution. The evolution of drug resistance begins in the microenvironment where MM cells receive the most protection from drug due to surrounding stromal cells and serum. As therapy is forced into the environment, cells begin mutating in a manner representative of natural selection. As mutations fail to protect cells outside of the perivascular niche, they are destroyed by therapeutic agents. However, once a path to successful resistance occurs through homologous MM-MM interaction or chromosomal

22

mutation, the cells being to survive irrespectively of niche location, causing EMDR score to drop as clustering occurs or highly complex, 'best fit', mutations occur within the cell. Another important finding suggests that development of resistance to a single agent is rarely the case. In fact, based on our results it is rare for cross-resistance not to occur, even to drugs that the patient has never been exposed to. This suggests that the evolution of drug resistance promotes such resistance in general, not necessarily to a predictable set of drugs. To make matters more complicated, each patient exhibits drug resistance evolution to different degrees through different mechanisms that result in different cross-resistances through time. It seems critical that precision medicine take hold to promote individualized therapy decisions for each patient afflicted with MM, bearing in mind that each line of therapy may promote resistance to others, even if they have remained foreign to the patient before that time.

These findings suggest that a change in perspective regarding therapy decision may be necessary to optimize patient response and limit relapse. Perhaps treatment at high concentration that more quickly removes the non-resistant cells will simply provide a more conducive environment for those MM cells that have established improved resistance phenotypes to grow more quickly. It may be more beneficial, therefore, to limit the number of drugs utilized over time and present them in concentrations that will manage the growth of sensitive cells and inhibit more evolutionarily fit subpopulations from taking over the tumoral space. Such therapy interventions may lead to less dramatic tumor burden reductions initially, but may also prevent the rapid and nearly inevitable relapse that occurs in MM patients today.
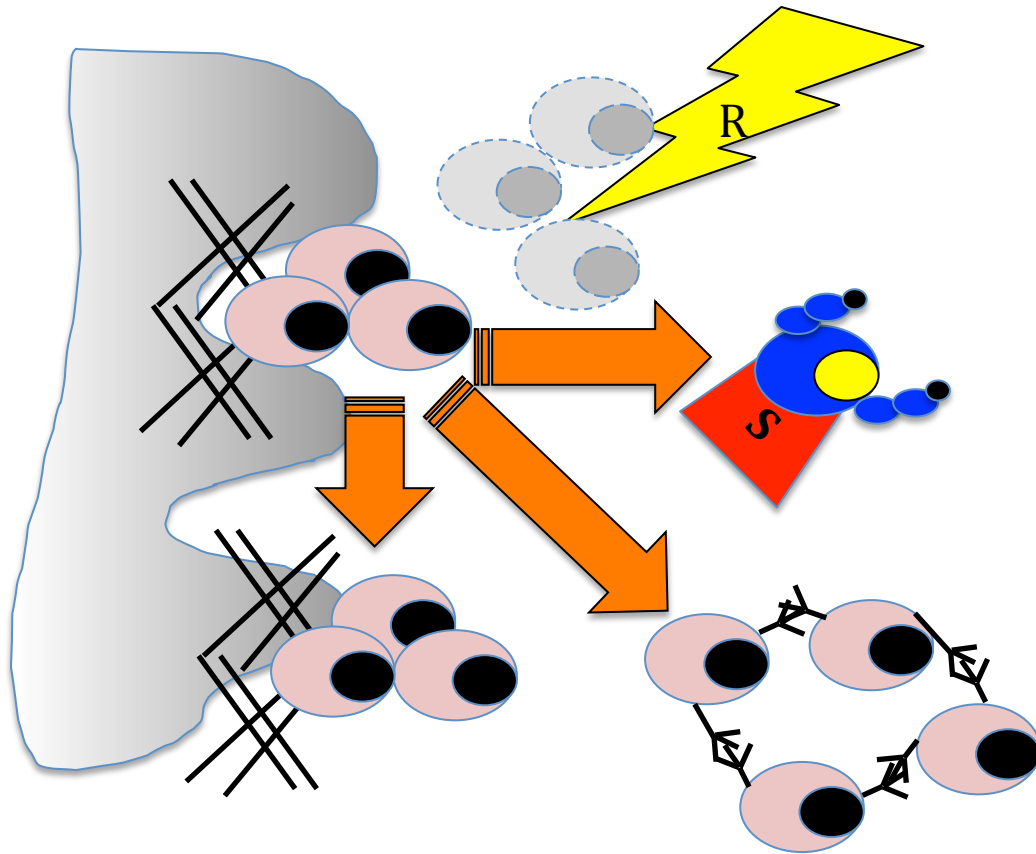
23

Figure 4.1: The Whole Picture: A Summary of Findings. Circles outlined in solid blue represent living MM, while the dashed line and gray inside represent those that have succumbed to therapy (yellow lightning bolt). Black lines on the left represent stromal cells in the perivascular niche and black 'fork' shapes between MM represent the signaling factors that promote MM-MM adhesion resistance. The blue cell represents successful genetic mutation that allows survival and drug resistance regardless of location, showing that the 'best' fit for evolutionary survival has been achieved and suggests that relapse will occur.

REFERENCES

1   Fadeev, R. S. *et al.* Cell Aggregation Increases Drug Resistance of Acute Myeloid Leukemia Cells. *Biol Membrany* **32**, 125-134, doi:10.7868/S0233475515020061 (2015).

2   Meads, M. B., Gatenby, R. A. & Dalton, W. S. Environment-mediated drug resistance: a major contributor to minimal residual disease. *Nature reviews. Cancer* **9**, 665-674, doi:10.1038/nrc2714 (2009).

3   Fonseca, R. *et al.* International Myeloma Working Group molecular classification of multiple myeloma: spotlight review. *Leukemia* **23**, 2210-2221, doi:10.1038/leu.2009.174 (2009).

4   Dewald, G. W., Kyle, R. A., Hicks, G. A. & Greipp, P. R. The clinical significance of cytogenetic studies in 100 patients with multiple myeloma, plasma cell leukemia, or amyloidosis. *Blood* **66**, 380-390 (1985).

5   Zandecki, M., Lai, J. L. & Facon, T. Multiple myeloma: almost all patients are cytogenetically abnormal. *Br J Haematol* **94**, 217-227 (1996).

6   Meads, M. B., Hazlehurst, L. A. & Dalton, W. S. The bone marrow microenvironment as a tumor sanctuary and contributor to drug resistance. *Clinical cancer research : an official journal of the American Association for Cancer Research* **14**, 2519-2526, doi:10.1158/1078-0432.CCR-07-2223 (2008).

7   Hazlehurst, L. A. & Dalton, W. S. Mechanisms associated with cell adhesion mediated drug resistance (CAM-DR) in hematopoietic malignancies. *Cancer metastasis reviews* **20**, 43-50 (2001).

8   Jean, C., Gravelle, P., Fournie, J. J. & Laurent, G. Influence of stress on extracellular matrix and integrin biology. *Oncogene* **30**, 2697-2706, doi:10.1038/onc.2011.27 (2011).

9   Tabernero, D. *et al.* Incidence of chromosome numerical changes in multiple myeloma: fluorescence in situ hybridization analysis using 15 chromosome-specific probes. *Am J Pathol* **149**, 153-161 (1996).

10   Avet-Loiseau, H. *et al.* Oncogenesis of multiple myeloma: 14q32 and 13q chromosomal abnormalities are not randomly distributed, but correlate with natural history, immunological features, and clinical presentation. *Blood* **99**, 2185-2191 (2002).

11   Drach, J. *et al.* Multiple myeloma: high incidence of chromosomal aneuploidy as detected by interphase fluorescence in situ hybridization. *Cancer Res* **55**, 3854-3859 (1995).

12   Fonseca, R. *et al.* Genetics and cytogenetics of multiple myeloma: a workshop report. *Cancer Res* **64**, 1546-1558 (2004).

13   Borrello, I. Can we change the disease biology of multiple myeloma? *Leuk Res* **36 Suppl 1**, S3-12, doi:10.1016/S0145-2126(12)70003-6 (2012).

14   Seidl, S., Kaufmann, H. & Drach, J. New insights into the pathophysiology of multiple myeloma. *Lancet Oncol* **4**, 557-564 (2003).

15   Chesi, M. *et al.* Frequent translocation t(4;14)(p16.3;q32.3) in multiple myeloma is associated with increased expression and activating mutations of fibroblast growth factor receptor 3. *Nat Genet* **16**, 260-264, doi:10.1038/ng0797-260 (1997).

16   Plowright, E. E. *et al.* Ectopic expression of fibroblast growth factor receptor 3 promotes myeloma cell proliferation and prevents apoptosis. *Blood* **95**, 992-998 (2000).

17   Martinez-Garcia, E. *et al.* The MMSET histone methyl transferase switches global histone methylation and alters gene expression in t(4;14) multiple myeloma cells. *Blood* **117**, 211-220, doi:10.1182/blood-2010-07-298349 (2011).

18   Avet-Loiseau, H. *et al.* Genetic abnormalities and survival in multiple myeloma: the experience of the Intergroupe Francophone du Myelome. *Blood* **109**, 3489-3495, doi:10.1182/blood-2006-08-040410 (2007).

19   Keats, J. J. *et al.* Clonal competition with alternating dominance in multiple myeloma. *Blood* **120**, 1067-1076, doi:10.1182/blood-2012-01-405985 (2012).

20   Hideshima, T., Mitsiades, C., Tonon, G., Richardson, P. G. & Anderson, K. C. Understanding multiple myeloma pathogenesis in the bone marrow to identify new therapeutic targets. *Nat Rev Cancer* **7**, 585-598, doi:10.1038/nrc2189 (2007).

21   Lohr, J. G. *et al.* Widespread genetic heterogeneity in multiple myeloma: implications for targeted therapy. *Cancer Cell* **25**, 91-101, doi:10.1016/j.ccr.2013.12.015 (2014).

22   Silva, A., Jacobson, T., Meads, M., Distler, A. & Shain, K. An Organotypic High Throughput System for Characterization of Drug Sensitivity of Primary Multiple Myeloma Cells. *J Vis Exp*, e53070, doi:10.3791/53070 (2015).

23   Meads, M. B., Hazlehurst, L. A. & Dalton, W. S. The bone marrow microenvironment as a tumor sanctuary and contributor to drug resistance. *Clin Cancer Res* **14**, 2519-2526, doi:10.1158/1078-0432.CCR-07-2223 (2008).

24   Hazlehurst, L. A. & Dalton, W. S. Mechanisms associated with cell adhesion mediated drug resistance (CAM-DR) in hematopoietic malignancies. *Cancer Metastasis Rev* **20**, 43-50 (2001).

25   Hazlehurst, L. A. *et al.* Reduction in drug-induced DNA double-strand breaks associated with beta1 integrin-mediated adhesion correlates with drug resistance in U937 cells. *Blood* **98**, 1897-1903 (2001).

26   Hazlehurst, L. A. *et al.* Cell adhesion to fibronectin (CAM-DR) influences acquired mitoxantrone resistance in U937 cells. *Cancer Res* **66**, 2338-2345, doi:10.1158/0008-5472.CAN-05-3256 (2006).

27   Shain, K. H., Landowski, T. H. & Dalton, W. S. Adhesion-mediated intracellular redistribution of c-Fas-associated death domain-like IL-1-converting enzyme-like inhibitory protein-long confers resistance to CD95-induced apoptosis in hematopoietic cancer cell lines. *J Immunol* **168**, 2544-2553 (2002).

28   Chauhan, D. *et al.* SHP2 mediates the protective effect of interleukin-6 against dexamethasone-induced apoptosis in multiple myeloma cells. *J Biol Chem* **275**, 27845-27850, doi:10.1074/jbc.M003428200 (2000).

29   Shain, K. H. *et al.* Beta1 integrin adhesion enhances IL-6-mediated STAT3 signaling in myeloma cells: implications for microenvironment influence on tumor survival and proliferation. *Cancer Res* **69**, 1009-1015, doi:10.1158/0008-5472.CAN-08-2419 (2009).

30   Damiano, J. S., Cress, A. E., Hazlehurst, L. A., Shtil, A. A. & Dalton, W. S. Cell adhesion mediated drug resistance (CAM-DR): role of integrins and resistance to apoptosis in human myeloma cell lines. *Blood* **93**, 1658-1667 (1999).

31   Reginato, M. J. *et al.* Integrins and EGFR coordinately regulate the pro-apoptotic protein Bim to prevent anoikis. *Nat Cell Biol* **5**, 733-740, doi:10.1038/ncb1026 (2003).

32   Juliano, R. L. Signal transduction by cell adhesion receptors and the cytoskeleton: functions of integrins, cadherins, selectins, and immunoglobulin-superfamily members. *Annu Rev Pharmacol Toxicol* **42**, 283-323, doi:10.1146/annurev.pharmtox.42.090401.151133 (2002).

33   Frieboes, H. B. *et al.* Prediction of drug response in breast cancer using integrative experimental/computational modeling. *Cancer Res* **69**, 4484-4492, doi:10.1158/0008-5472.CAN-08-3740 (2009).

34   Cristini, V. *et al.* Morphologic instability and cancer invasion. *Clin Cancer Res* **11**, 6772-6779, doi:10.1158/1078-0432.CCR-05-0852 (2005).

35   Sinek, J. P. *et al.* Predicting drug pharmacokinetics and effect in vascularized tumors using computer simulation. *J Math Biol* **58**, 485-510, doi:10.1007/s00285-008-0214-y (2009).

36   Grantab, R. H. & Tannock, I. F. Penetration of anticancer drugs through tumour tissue as a function of cellular packing density and interstitial fluid pressure and its modification by bortezomib. *BMC Cancer* **12**, 214, doi:10.1186/1471-2407-12-214 (2012).

37   Laurent, J. *et al.* Multicellular tumor spheroid models to explore cell cycle checkpoints in 3D. *BMC Cancer* **13**, 73, doi:10.1186/1471-2407-13-73 (2013).

38   Dai, Y. & Grant, S. New Insights into Checkpoint Kinase 1 in the DNA Damage Response Signaling Network. *Clinical Cancer Research* **16**, 376-383, doi:10.1158/1078-0432.Ccr-09-1029 (2010).

39   Malumbres, M. & Barbacid, M. Cell cycle, CDKs and cancer: a changing paradigm. *Nature Reviews Cancer* **9**, 153-166, doi:10.1038/nrc2602 (2009).

40   Bartl, R. Histologic classification and staging of multiple myeloma. *Hematol Oncol* **6**, 107-113 (1988).

41   Derksen, P. W. *et al.* Illegitimate WNT signaling promotes proliferation of multiple myeloma cells. *Proc Natl Acad Sci U S A* **101**, 6122-6127, doi:10.1073/pnas.0305855101 (2004).

42   Derycke, L. D. & Bracke, M. E. N-cadherin in the spotlight of cell-cell adhesion, differentiation, embryogenesis, invasion and signalling. *Int J Dev Biol* **48**, 463-476, doi:10.1387/ijdb.041793ld (2004).

43   Groen, R. W. *et al.* N-cadherin-mediated interaction with multiple myeloma cells inhibits osteoblast differentiation. *Haematologica* **96**, 1653-1661, doi:10.3324/haematol.2010.038133 (2011).

44   Bergsagel, P. L. *et al.* Cyclin D dysregulation: an early and unifying pathogenic event in multiple myeloma. *Blood* **106**, 296-303, doi:10.1182/blood-2005-01-0034 (2005).

45   Khin, Z. P. *et al.* A preclinical assay for chemosensitivity in multiple myeloma. *Cancer Res* **74**, 56-67, doi:10.1158/0008-5472.CAN-13-2397 (2014).

46   Silva, A., Jacobson, T., Meads, M., Distler, A. & Shain, K. An Organotypic High Throughput System for Characterization of Drug Sensitivity of Primary Multiple Myeloma Cells. *J. Vis. Exp.* **e53070**, doi:10.3791/53070 (2015).

47   Lohr, J. G. *et al.* Widespread genetic heterogeneity in multiple myeloma: implications for targeted therapy. *Cancer cell* **25**, 91-101, doi:10.1016/j.ccr.2013.12.015 (2014).

48   Kitano, H. The theory of biological robustness and its implication in cancer. *Ernst Schering Research Foundation workshop*, 69-88 (2007).

27

49   Uchiyama, H., Barut, B. A., Mohrbacher, A. F., Chauhan, D. & Anderson, K. C. Adhesion of human myeloma-derived cell lines to bone marrow stromal cells stimulates interleukin-6 secretion. *Blood* **82**, 3712-3720 (1993).

50   Catlett-Falcone, R. *et al.* Constitutive activation of Stat3 signaling confers resistance to apoptosis in human U266 myeloma cells. *Immunity* **10**, 105-115 (1999).

51   Brocke-Heidrich, K. *et al.* Interleukin-6-dependent gene expression profiles in multiple myeloma INA-6 cells reveal a Bcl-2 family-independent survival pathway closely associated with Stat3 activation. *Blood* **103**, 242-251, doi:10.1182/blood-2003-04-1048 (2004).

52   Puthier, D., Bataille, R. & Amiot, M. IL-6 up-regulates mcl-1 in human myeloma cells through JAK / STAT rather than ras / MAP kinase pathway. *Eur J Immunol* **29**, 3945-3950 (1999).

53   Hu, L. *et al.* Downstream effectors of oncogenic ras in multiple myeloma cells. *Blood* **101**, 3126-3135, doi:10.1182/blood-2002-08-2640 (2003).

54   Meads, M. B., Gatenby, R. A. & Dalton, W. S. Environment-mediated drug resistance: a major contributor to minimal residual disease. *Nat Rev Cancer* **9**, 665-674, doi:10.1038/nrc2714 (2009).

55   Hazlehurst, L. A., Argilagos, R. F. & Dalton, W. S. Beta1 integrin mediated adhesion increases Bim protein degradation and contributes to drug resistance in leukaemia cells. *Br J Haematol* **136**, 269-275, doi:10.1111/j.1365-2141.2006.06435.x (2007).

56   Hazlehurst, L. A., Damiano, J. S., Buyuksal, I., Pledger, W. J. & Dalton, W. S. Adhesion to fibronectin via beta1 integrins regulates p27kip1 levels and contributes to cell adhesion mediated drug resistance (CAM-DR). *Oncogene* **19**, 4319-4327, doi:10.1038/sj.onc.1203782 (2000).

57   Nefedova, Y., Landowski, T. H. & Dalton, W. S. Bone marrow stromal-derived soluble factors and direct cell contact contribute to de novo drug resistance of myeloma cells by distinct mechanisms. *Leukemia* **17**, 1175-1182, doi:10.1038/sj.leu.2402924 (2003).

58   Croix, B. S. *et al.* Reversal by hyaluronidase of adhesion-dependent multicellular drug resistance in mammary carcinoma cells. *J Natl Cancer Inst* **88**, 1285-1296 (1996).

59   Bellamy, W. T., Dalton, W. S., Gleason, M. C., Grogan, T. M. & Trent, J. M. Development and characterization of a melphalan-resistant human multiple myeloma cell line. *Cancer Res* **51**, 995-1002 (1991).

60   Abdi, J., Chen, G. & Chang, H. Drug resistance in multiple myeloma: latest findings and new concepts on molecular mechanisms. *Oncotarget* **4**, 2186-2207, doi:10.18632/oncotarget.1497 (2013).

61   Levenberg, S., Yarden, A., Kam, Z. & Geiger, B. p27 is involved in N-cadherin-mediated contact inhibition of cell growth and S-phase entry. *Oncogene* **18**, 869-876, doi:10.1038/sj.onc.1202396 (1999).

62   Albert, D. H. *et al.* Preclinical activity of ABT-869, a multitargeted receptor tyrosine kinase inhibitor. *Mol Cancer Ther* **5**, 995-1006, doi:10.1158/1535-7163.MCT-05-0410 (2006).

63   Levis, M. *et al.* A FLT3-targeted tyrosine kinase inhibitor is cytotoxic to leukemia cells in vitro and in vivo. *Blood* **99**, 3885-3891 (2002).

64   Hernandez-Davies, J. E. *et al.* The Multitargeted Receptor Tyrosine Kinase Inhibitor Linifanib (ABT-869) Induces Apoptosis through an Akt and Glycogen Synthase Kinase 3 beta-Dependent Pathway. *Molecular Cancer Therapeutics* **10**, 949-959, doi:10.1158/1535-7163.Mct-10-0904 (2011).

29

APPENDIX A: SUPPLEMENTAL FIGURES

Below are figures comprising all data collected for the seven patient cases analyzed in this manuscript. N/A signifies that the data was unavailable for collection, not excluded for ulterior means.
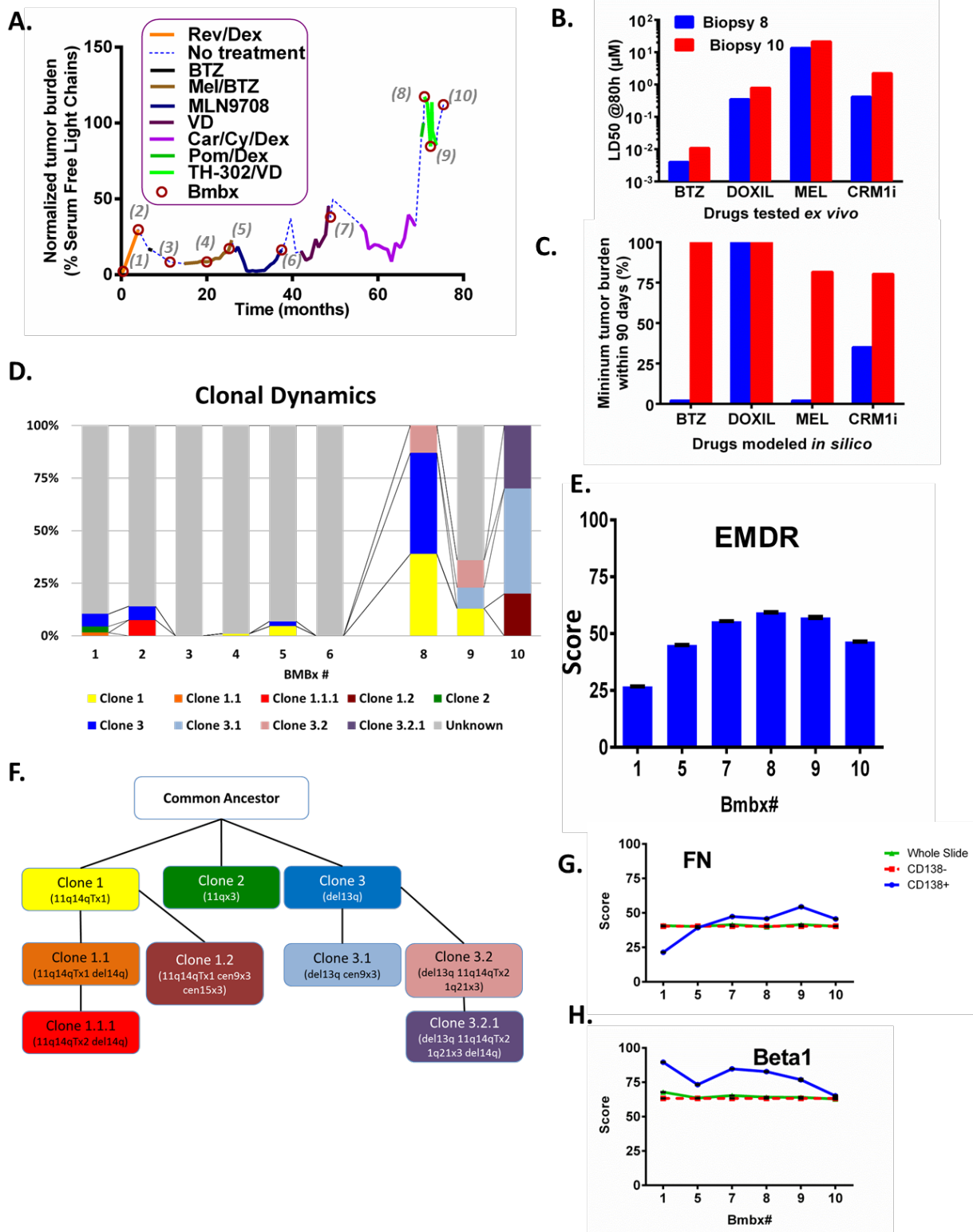
**Figure A.1: Case 1 Patient History, Ex Vivo Results, FISH, and EMDR.**
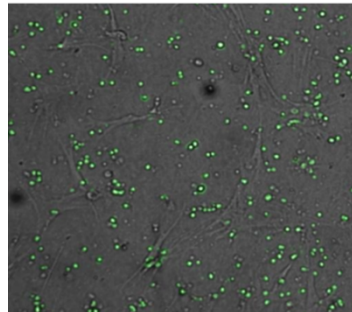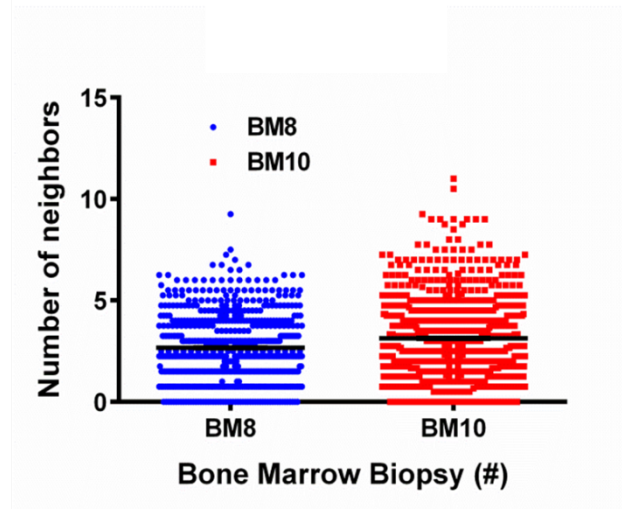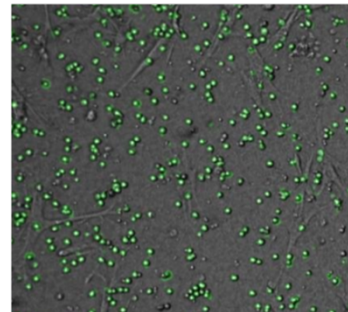
Figure A.2: Case 1 Clustering Analysis Results.
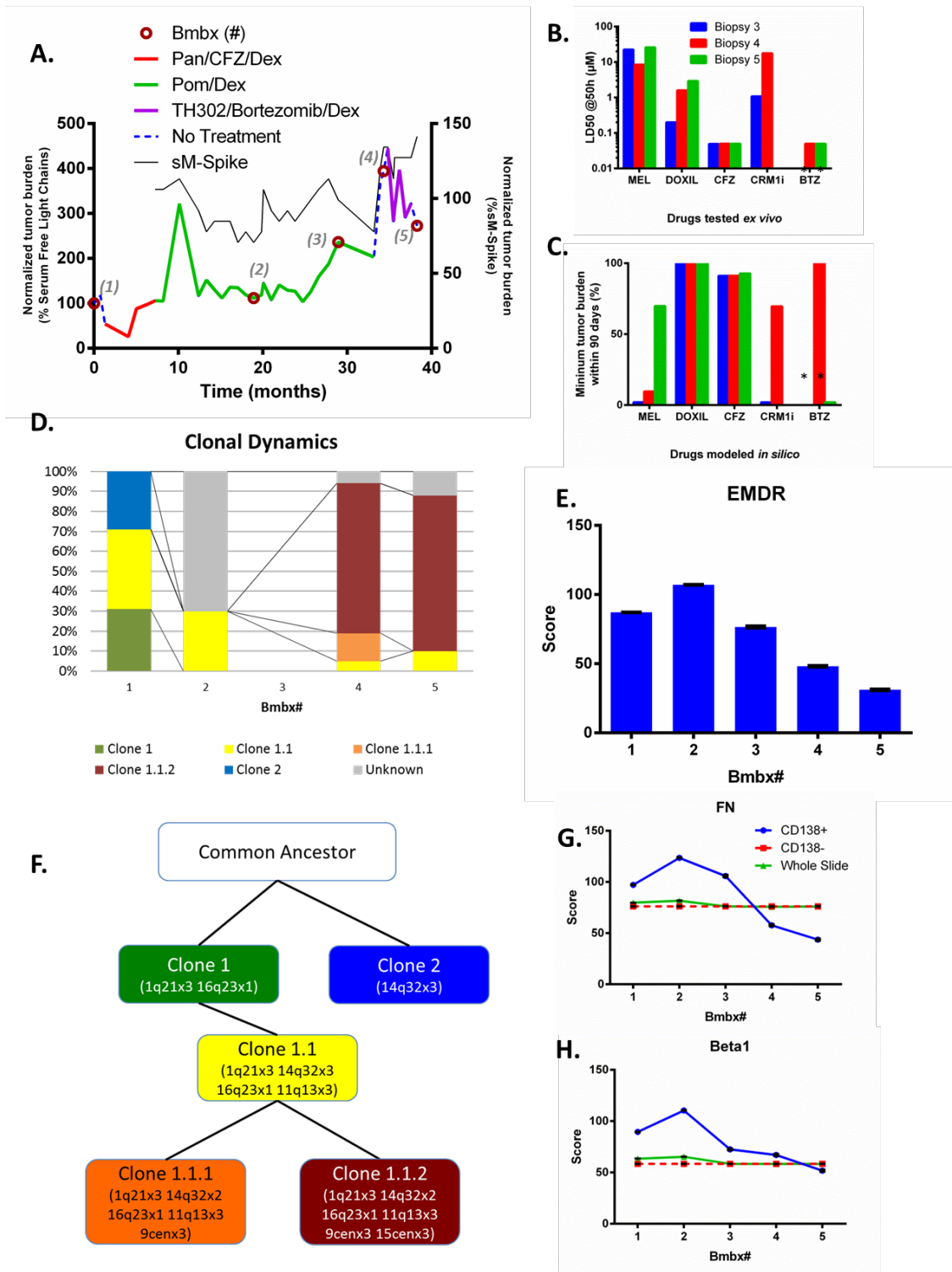
Figure A.3: Case 2 Patient History, Ex Vivo Results, FISH, and EMDR.
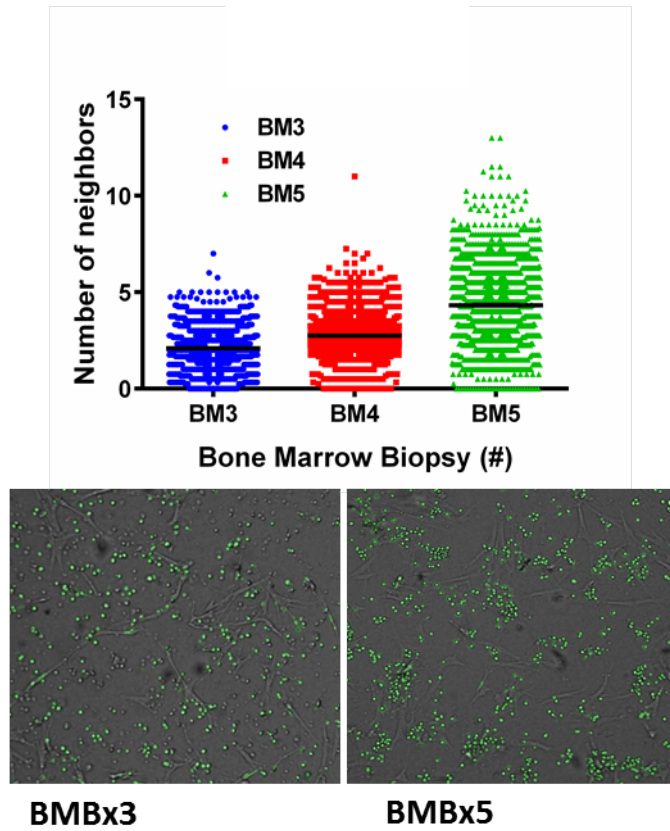
Figure A.4: Case 2 Clustering Analysis Results.
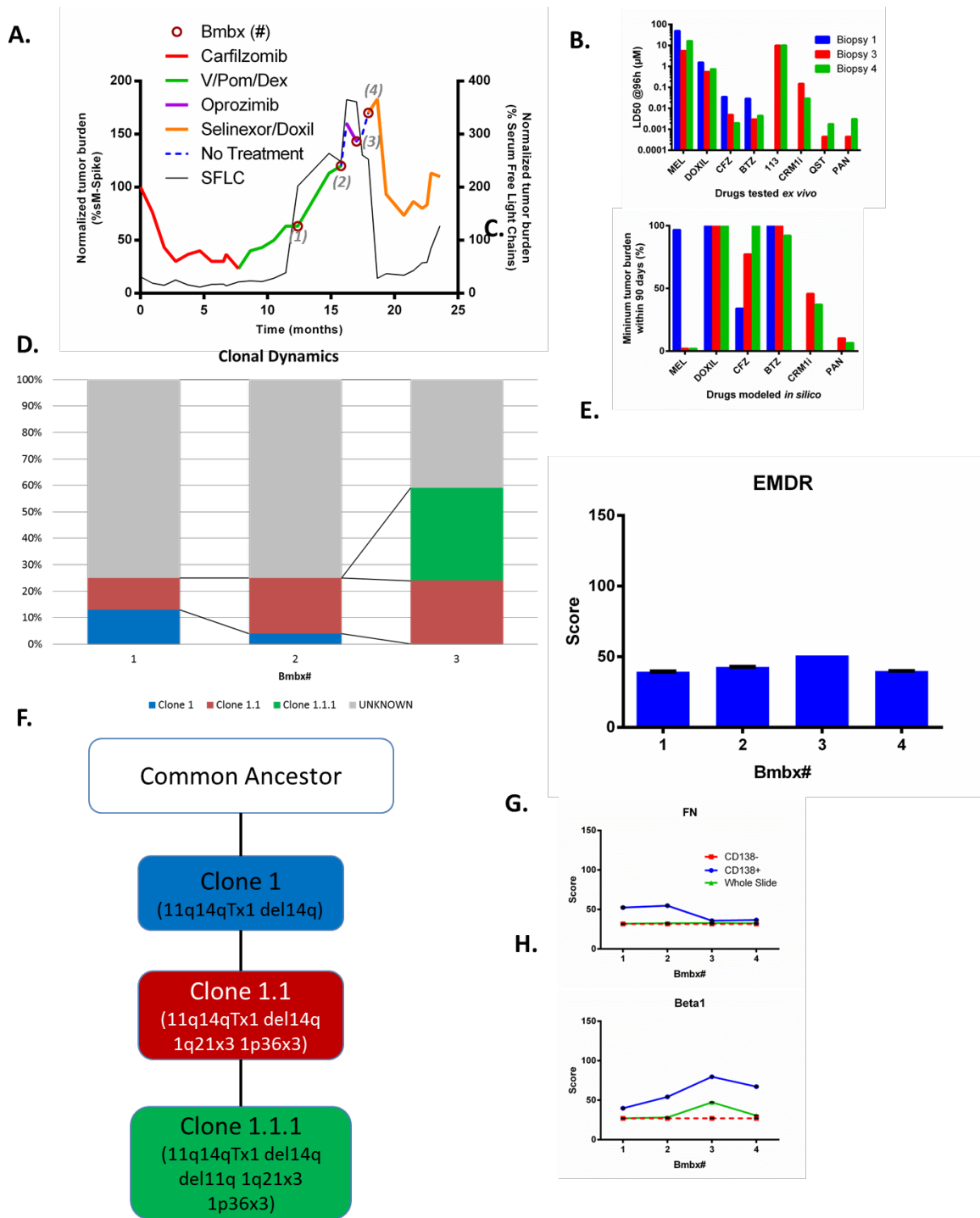
Figure A.5: Case 3 Patient History, Ex Vivo Results, FISH, and EMDR.
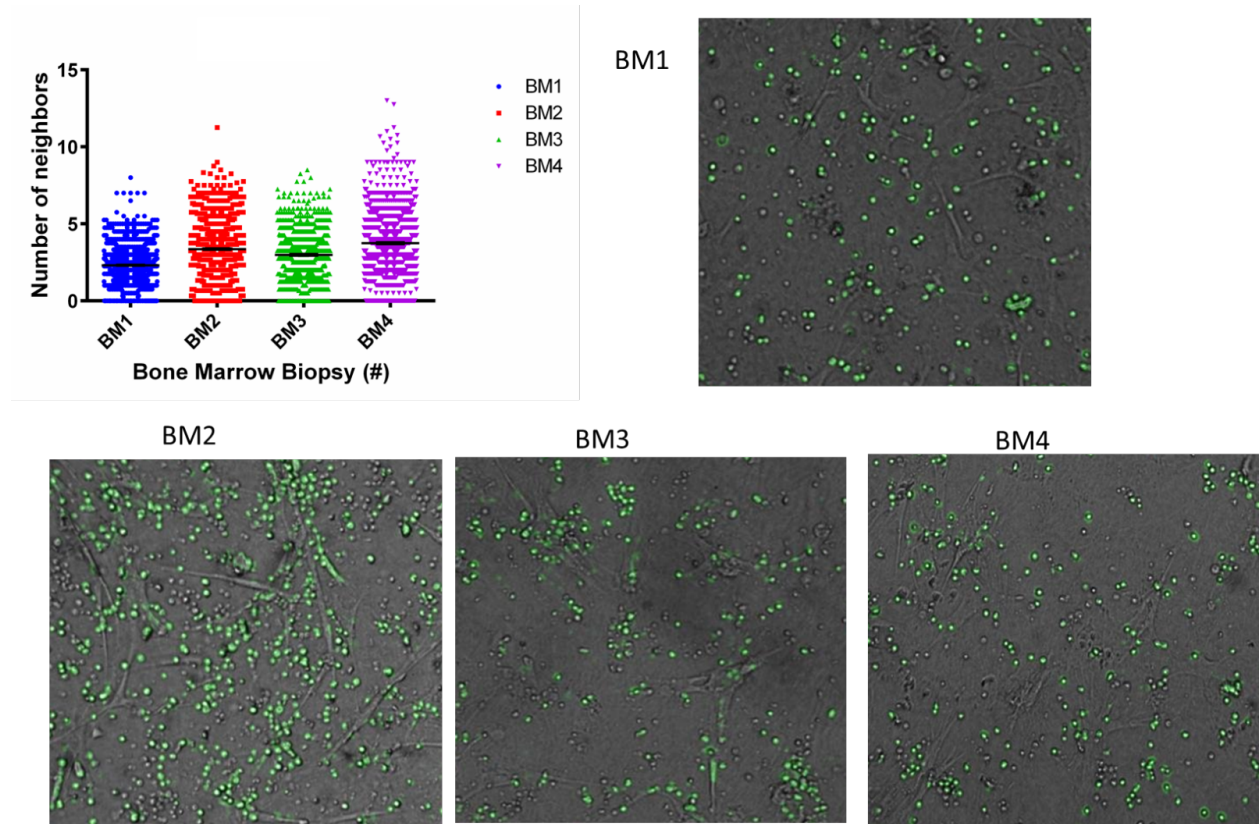
Figure A.6: Case 3 Clustering Analysis Results.
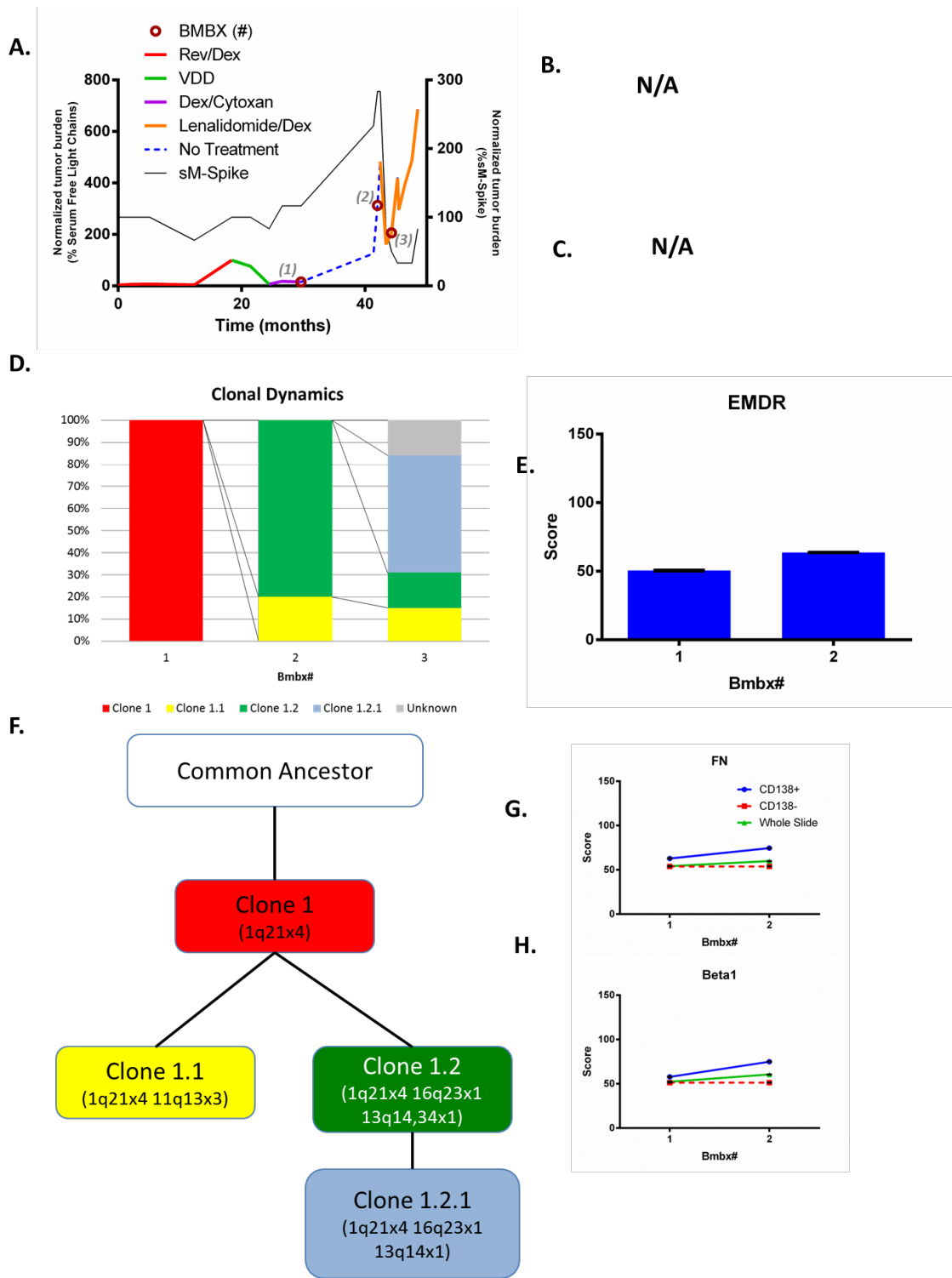
Figure A.7: Case 4 Patient History, FISH, and EMDR.
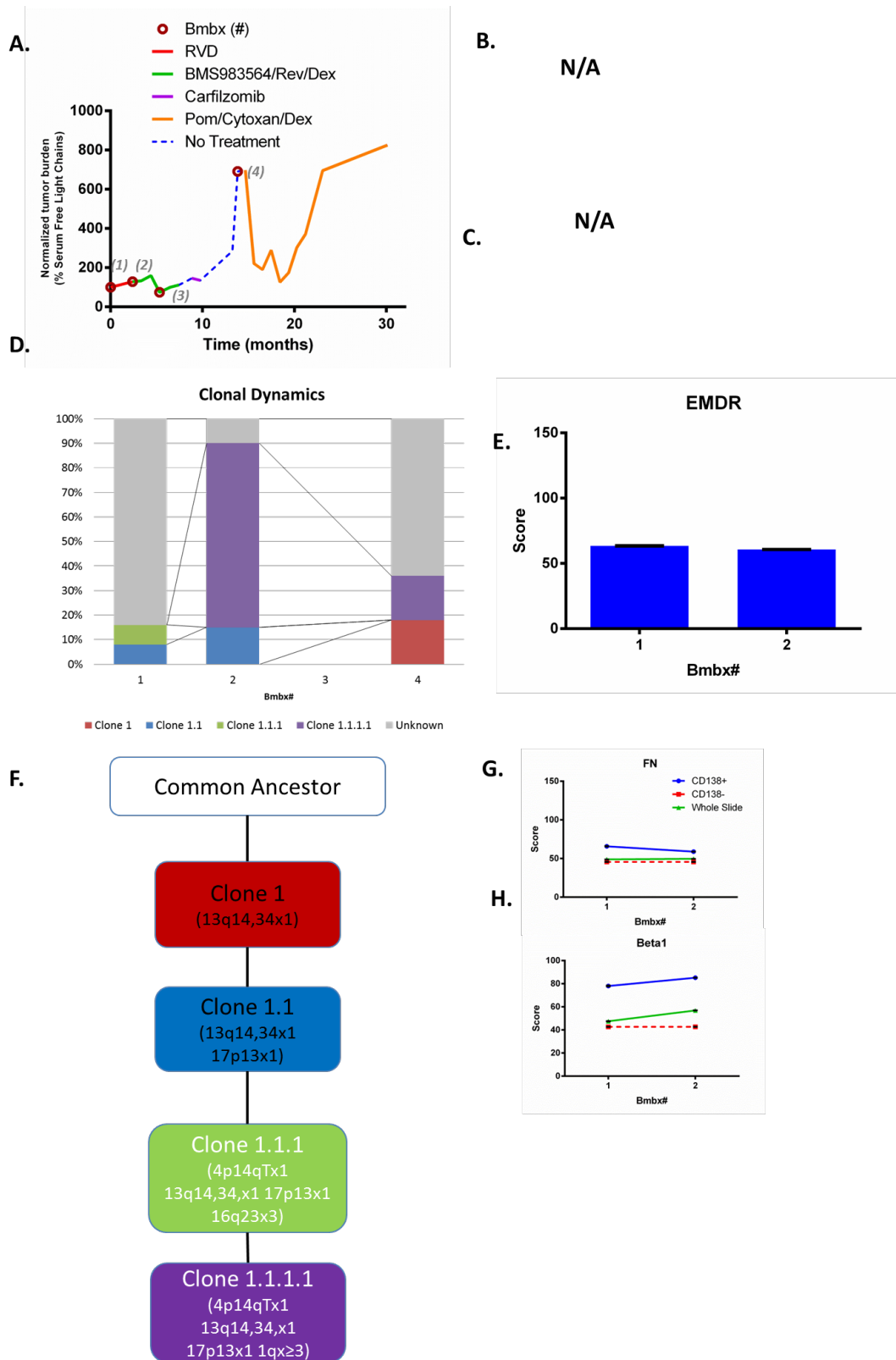
Figure A.8: Case 5 Patient History, FISH, and EMDR.
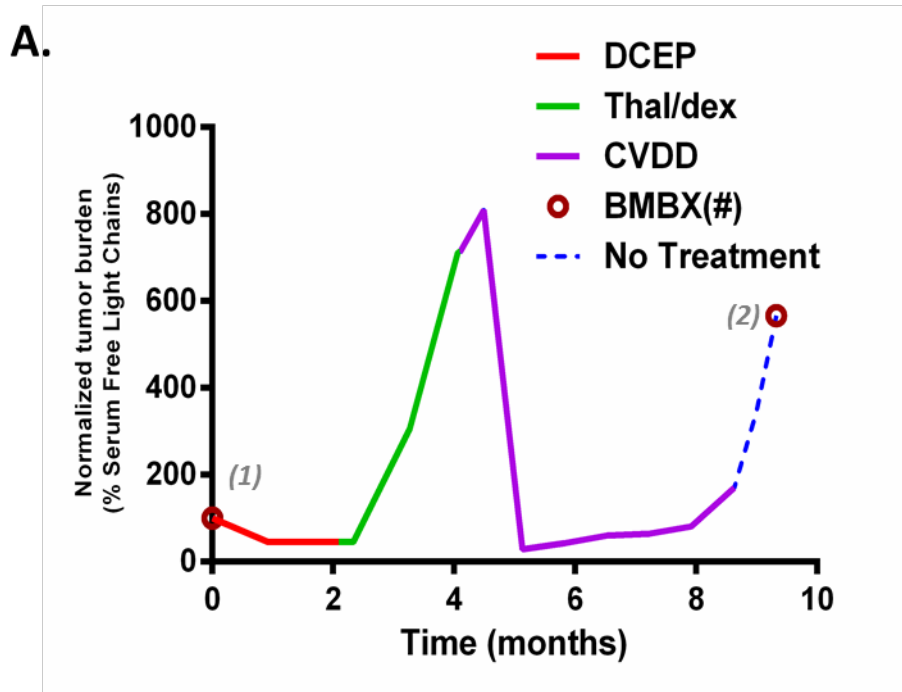
Figure A.9: Case 6 Patient History.
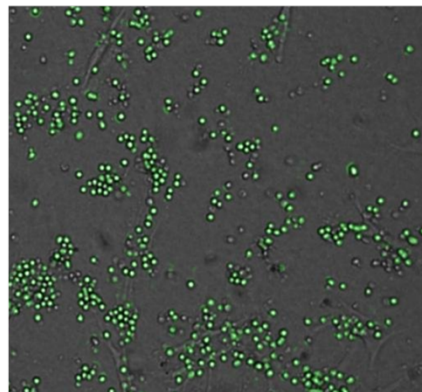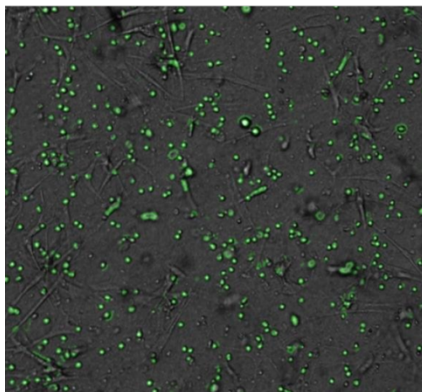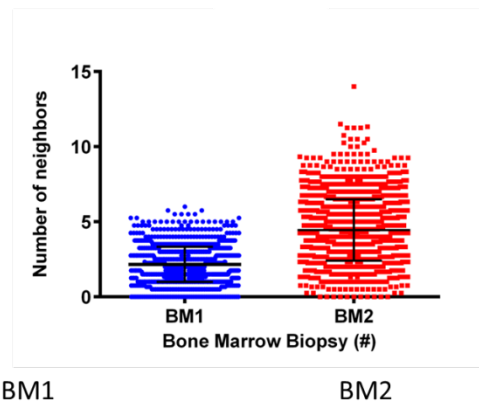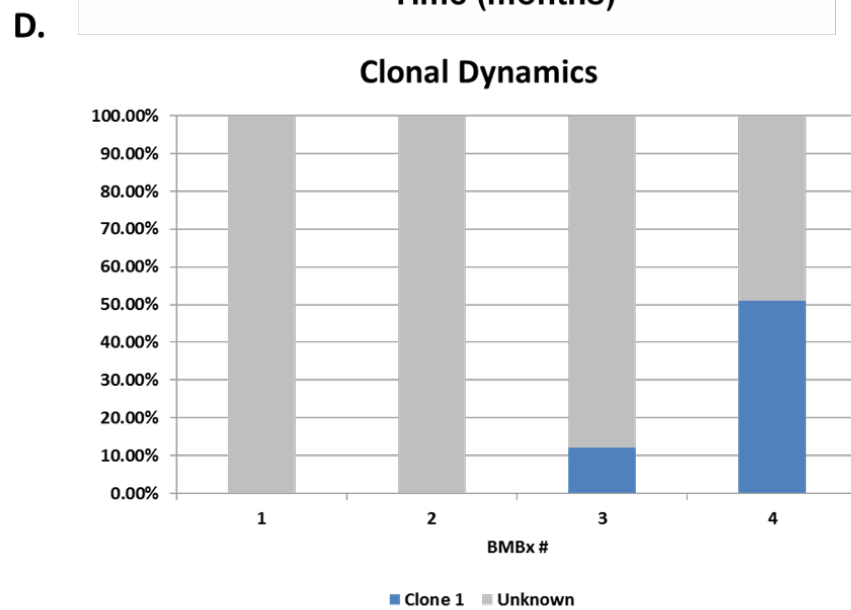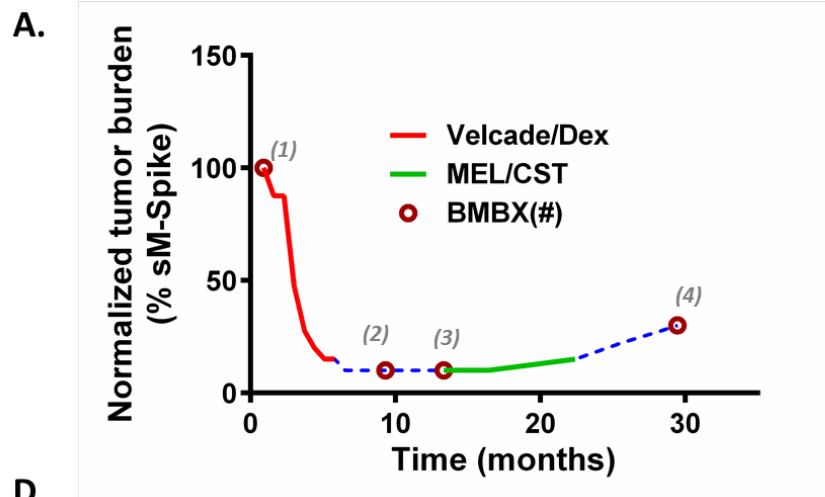

Figure A.10: Case 6 Clustering Analysis Results.
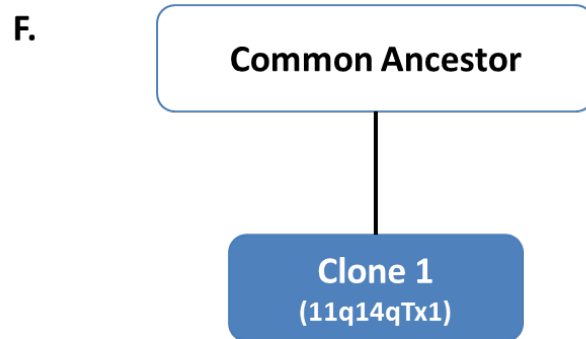
Figure A.11: Case 7 Patient History and FISH.